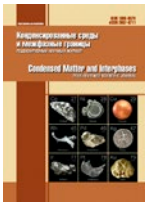

ISSN 1606-867X (Print)
ISSN 2687-0711 (Online)
Condensed Matter and Interphases
Kondensirovannye Sredy i Mezhfaznye Granitsy
https://journals.vsu.ru/kcmf/

Original articles

Research article
https://doi.org/10.17308/kcmf.2024.26/11811

An investigation of the electronic structure and optoelectronic properties of 4-((2-hydroxy-3-methoxybenzylidene)amino)-N-(thiazol-2-yl) benzene sulfonamide

D. M. Mamand[1], D. M. Aziz[2], H. M. Qadr[1]✉

[1]*University of Raparin, College of Science, Department of Physics, Sulaymaniyah, Iraq*

[2]*University of Raparin, College of Science, Department of Chemistry, Sulaymaniyah, Iraq*

Abstract

Molecules of 4-((2-hydroxy-3-methoxybenzylidene)amino)-N-(thiazol-2-yl)benzene sulfonamide were investigated at varying concentrations in dimethyl sulfoxide (DMSO). Different temperatures were employed to assess bandgap energies, Tauc plots, refractive indices, optical and electrical properties, and dielectric constants. The refractive index was determined through a straightforward model based on energy gap data and subsequently compared to experimental values. For the examination of the materials' optical properties, reflection and reflection loss at plasma frequencies were considered as they play a crucial role. Density functional theory (DFT) with a 6-311G++ (d, p) basis set and Becke's three-parameter hybrid (B3LYP) level of theory were utilized through Gaussian software to conduct the studies. Chemical reactivity and selectivity parameters, including HOMO-LUMO, global hardness, softness, electronegativity, electrophilicity, nucleophilicity, chemical potential, bandgap energy, and electron affinity, were computed. Becke's three-parameter hybrid exchange-correlation functional (B3LYP) level was employed for optimizing the geometry of the title molecule.

Keywords: Optoelectronic, UV-visible spectroscopy, HOMO-LUMO, DFT

For citation: Mamand D. M., Aziz D. M., Qadr H. M. An investigation of the electronic structure and optoelectronic properties of 4-((2-hydroxy-3-methoxybenzylidene) amino)-N-(thiazol-2-yl) benzene sulfonamide. *Condensed Matter and Interphases*. 2024;26(1): 88–103. https://doi.org/10.17308/kcmf.2024.26/11811

Для цитирования: Маманд Д. М., Азиз Д. М., Квадр Х. М. Исследование электронной структуры и оптоэлектронных свойств 4-((2-гидрокси-3-метоксибензилиден)амино)-N-(тиазол-2-ил) бензолсульфонамида. *Конденсированные среды и межфазные границы*. 2024;26(1): 88–103. https://doi.org/10.17308/kcmf.2024.26/11811

✉ Hiwa M. Qadr, e-mail: hiwa.physics@uor.edu.krd
© Mamand D. M., Aziz D. M., Qadr H. M., 2024

The content is available under Creative Commons Attribution 4.0 License.

1. Introduction

Numerous biodegradable materials, including those designed for electronic applications, hold potential for utilization in the fabrication of electronic devices. Through the application of optical absorption spectroscopy, the optical and electronic characteristics of these biomaterials have been investigated, providing insights into energy diagrams, energy band gaps, and optoelectronic properties associated with such materials [1–3]. The majority of biomaterials, including those with bandgap energies exceeding 2.5 eV such as gelatin, glycerol, and fibrinogen, have been previously documented in studies with values of 3, 3.54, and 3.02 eV, respectively [4–7]. Semiconductor materials typically exhibit bandgap energies falling within the range of 1–1.5 eV, exemplified by conventional semiconductors like gallium arsenide and silicon[8]. In contrast, wide-bandgap (WBG) semiconductors, characterized by bandgaps ranging from 2 to 4 eV, possess distinctive properties that enable devices to operate at higher voltages, frequencies, and temperatures compared to conventional semiconductors [9, 10]. For the investigation of optoelectronic properties, key parameters include bandgap energy, Tauc plot, refractive index, transmittance of light through the molecule, and dielectric properties [11, 12]. The refractive index, an optical property describing the relative speed of light through a material, is influenced by the material's crystalline structure and density, providing valuable physical and chemical characteristics for characterization[13, 14]. With diverse applications in fields such as the pharmaceutical industry, the refractive index plays a crucial role. This study focuses on the theoretical and experimental examination of the molecule 4-((2-hydroxy-3-methoxybenzylidene) amino)-N-(thiazol-2-yl)benzene sulfonamide in dimethyl sulfoxide (DMSO). The investigation aims to determine the applicability of this newly synthesized molecule by assessing physicochemical properties, including physical properties, solvation properties related to interactions with different media, and intrinsic chemical reactivity[15–18]. In recent years, the consideration of physical and chemical characteristics of drugs has gained prominence, as these properties significantly influence a chemical compound's pharmacological and therapeutic effects. The action and responsivity of a drug can be correlated with its physical and chemical properties, encompassing neutralization, chelation, oxidation, and extracellular reactions [19, 20]. Given the advantages of photonics in various industries, such as optical communications, data storage, and image processing, there is growing interest in nonlinear optical reactions in diverse materials [21].

The primary objective of this study is to comprehensively examine the chemical, physical, and optoelectronic properties of the newly synthesized molecule, including a fully optimized geometrical structure (refer to Figs. 1 and 2) [22]. Quantitative calculations based on Density Functional Theory (DFT) were employed to determine the electronic structure and several quantitative chemical parameters.

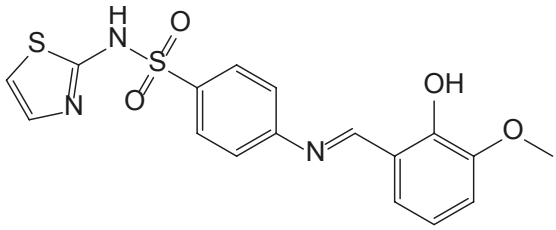

Fig. 1. Chemical structure of 4-((2-hydroxy-3-methoxybenzylidene) amino)-N-(thiazole-2-yl) benzene-sulfonamide

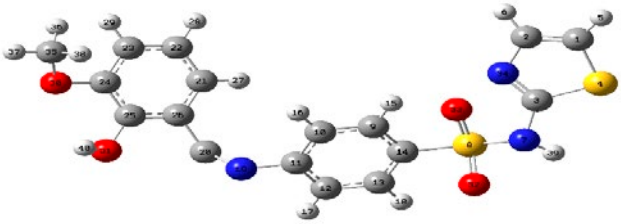

Fig. 2. Optimized structure

2. UV-visible spectroscopy

UV-visible spectroscopy stands out as a highly valuable and straightforward optical technique for probing the optical and electrical properties of nanomaterials. Numerous research endeavors have harnessed the power of UV-visible applications to elucidate the behavior of diverse nanomaterials, ranging from polymers and organic light-emitting materials to combinations of organic and inorganic semiconductors[23,

24]. The reflected spectra obtained through this technique offer insights into the fundamental electronic properties of the samples under investigation. The bandgap energy, a crucial parameter, plays a pivotal role in defining various optical properties such as refractive index, scattering angular frequency, electronegativity, and dielectric constant of materials. This parameter has emerged as a powerful tool for efficiently designing novel semiconductor devices, including 2D electron gas and LEDs [25]. Notably, the bandgap energy of materials has recently gained recognition not only in the context of advanced semiconductor technology but also in the construction of cutting-edge equipment. This recognition extends to its role as a technology platform facilitating the development of innovative devices like high-capacity batteries and ultra-efficient solar cells [25]. In scenarios involving embedded electric fields, the technique proves essential for ionizing holes from deep acceptor dopants. This ionization process is facilitated by the unbalanced polarization charge correlated with the gradient layer, thereby enabling the creation of electric fields. The material 4-((2-hydroxy-3-methoxybenzylidene) amino)-N-(thiazol-2-yl)benzene sulfonamide, and materials derived from it, can be applied to semiconductor crystals capable of maintaining sufficient piezoelectric polarization and strong spontaneous polarization. These properties make them versatile candidates for a range of applications in the realm of nanoelectronics and advanced semiconductor devices.

The relationship between the absorbance of light at a specific frequency and the concentration of molecules is found to be directly proportional, as illustrated in Table 1. This association is further elucidated in Fig. 3, where an increase in the absorption of photon energy is observed in tandem with changes in concentration, akin to the effect of path length. The initial concentration of the solution is highest, resulting in a greater number of molecules for incident light to interact with as it traverses through the medium. Consequently, an elevated concentration leads to increased light absorption, signifying a higher number of molecules in the solution. This alignment with Beer-Lambert's law establishes a direct proportionality between absorbance and concentration, where an augmentation in the original concentration corresponds to an increase in absorption.

Table. 1. Maximum absorption at different concentrations and temperatures 4-((2-hydroxy-3-methoxybenzylidene) amino)-N-(thiazole-2-yl) benzenesulfonamide in DMSO

	Temperature 303.15 K			Temperature 313.15 K		
Concentration (mg/l)	1. 026	0.513	0.2565	1. 026	0.513	0.2565
λ_{max} (nm)	362	331	328	362	353	325.32
Bandgap (eV)	3.425	3.746	3.78	3.425	3.512	3.811

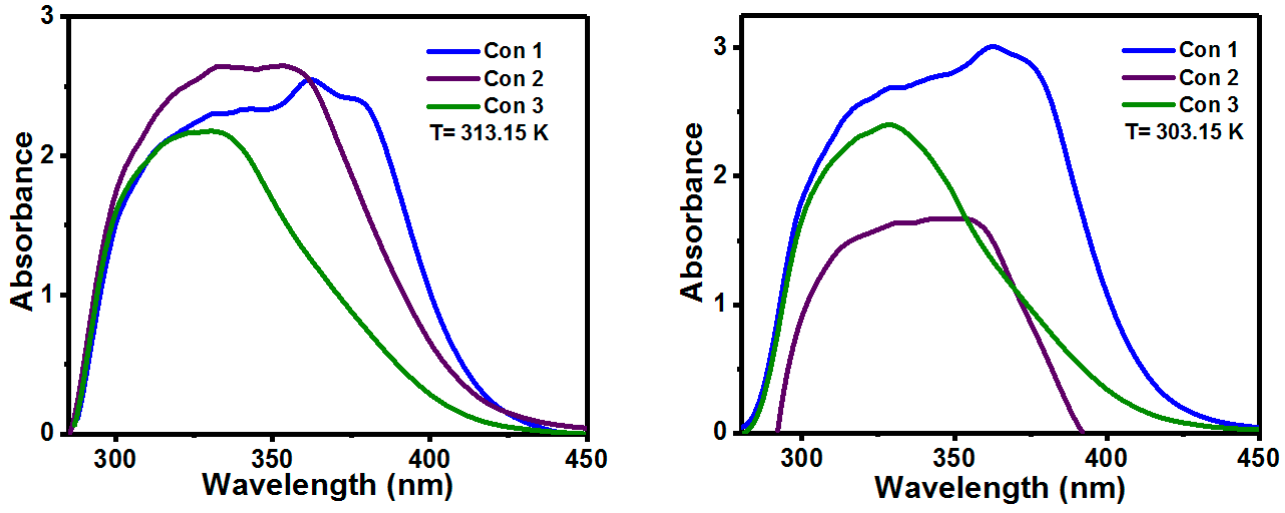

Fig. 3. UV-spectrum of 4-((2-hydroxy-3-methoxybenzylidene) amino)-N-(thiazol-2-yl) benzene sulfonamide in DMSO solvent at different temperatures

However, the second concentration exhibits a decrease in absorption. This deviation can be rationalized by considering the dilution of the solution, implying a reduction in the initial concentration. As the solution is diluted, the number of molecules available for light interaction decreases, resulting in a proportional decrease in absorption. This observation aligns with Beer-Lambert's law, emphasizing the direct relationship between absorbance and concentration. Therefore, in the present study, the reduction in absorption at the second concentration level can be attributed to the dilution of the solution, reflecting the anticipated proportional decrease in concentration.

The optical and electrical characteristics of semiconductor materials exhibit notable distinctions between wide bandgap energies and narrow bandgap energy configurations. The molecule 4-((2-hydroxy-3-methoxybenzylidene) amino)-N-(thiazol-2-yl)benzene sulfonamide possesses a wide bandgap exceeding 3 eV. Wide-bandgap semiconductors (WBGSs) are characterized by a larger bandgap compared to conventional semiconductors, with the latter falling within the 1-1.5 eV range (e.g., germanium and silicon), while the former extends from 2 to 4 eV. Typically, WBGSs exhibit electronic characteristics intermediate to insulators and conventional semiconductors. The distinct properties of WBGS materials make them highly suitable for a broad spectrum of applications, allowing devices to operate at significantly elevated voltages, frequencies, and temperatures, approximately up to 300 °C. This capability surpasses the operational limits of conventional semiconductor materials like silicon and gallium arsenide. Applications utilizing WBGS materials include a variety of devices and pigments such as radars, radiofrequency devices, lasers, and light-emitting diodes (LEDs), benefitting from their ability to function at higher power levels under normal conditions due to their enhanced thermal stability [26-28]. The electronic spectra of the 4-((2-hydroxy-3-methoxybenzylidene) amino)-N-(thiazol-2-yl)benzene sulfonamide compound reveal two discernible bands. The first band, located at λ_{max} = 300–312 nm, is attributed to the $^{*}\pi \rightarrow \pi$ transition within the aromatic system of the phenyl group. The third band, situated at λ_{max} = 430–460 nm, is associated with the C=N chromophore of these compounds, as indicated in Table 1. UV–visible spectra of this compound were investigated at different temperatures in dimethyl sulfoxide (DMSO), with Figure 3 depicting the UV spectra of compound at varying temperatures. At room temperature, the selected compound exhibits two absorptions in the range of 300–600 nm, specifically at 393 nm for the enol-imine form and at 453 nm for the keto-amine form. Upon cooling the solution to 15 °C, a color change from orange to yellow occurs, accompanied by the disappearance of the absorption band at 453 nm for the keto form in the UV–visible spectra. Upon reheating the solution, the absorption band for the keto form reappears. This behavior indicates the existence of an enol–keto equilibrium, and notably, the equilibrium is temperature-dependent.

This study aims to explore the optoelectronic properties of the 4-((2-hydroxy-3-methoxybenzylidene)amino)-N-(thiazol-2-yl)benzenesulfonamide molecule, garnering significant interest due to its noteworthy optical characteristics. The bandgap energy of this molecule is assessed through UV calculations, as depicted in Figures 2 and 3. The UV spectra reveal a singular peak across various concentrations and temperatures, as detailed in Table 1. The substantial bandgap within this range makes it particularly intriguing for applications in optoelectronic devices and transparent conductive oxide electrodes within solar cells. The utility of bandgap energy in this context is vital for extracting photo-generated carriers in solar cells. Transparent conducting oxide semiconductors, especially those with continuously graded bandgaps, have become a focal point of interest [29]. The ability to tune bandgap energy through continuous and independent manipulation of hole and electron properties adds versatility to its potential applications. The classification of optical bandgap is a prerequisite for device fabrication and holds significance in the optical characterization of these applications. Understanding and manipulating the bandgap energy of the 4-((2-hydroxy-3-methoxybenzylidene)amino)-N-(thiazol-2-yl)benzenesulfonamide molecule offer promising avenues for advancing optoelectronic

technologies, paving the way for innovative developments in solar cells and related devices.

3. Tauc-plot calculations

The absorption coefficient (α) with respect to photon energy ($h\nu$) serves as a metric for characterizing the light absorption properties of semiconductor materials. The provided expression facilitates the computation of both the optical bandgap energy (E_g) and the forbidden bandwidth associated with optical transitions in semiconductors. This formalism enables the determination of key parameters critical for understanding the semiconductor's response to light absorption, offering insights into its optical behavior and facilitating the calculation of optical bandgap energy and forbidden bandwidth E_g [30]:

$$(\alpha h\nu) = A^* (h\nu - E_g)^m . \quad (1)$$

Here, A^* denotes a constant, and m serves as the parameter associated with the characterization of band gaps based on the measurement type. For any transition to occur, the principles of crystal momentum conservation and energy conservation must be adhered to. In semiconductor physics, the bandgap of a semiconductor encompasses two distinct types: direct and indirect bandgaps. The maximal-energy state in the valence band and the minimal energy state in the conduction band within the Brillouin zone are distinctly characterized by specific crystal momentum [31]. The term "indirect bandgap" is applied when the crystal momentum of electrons and holes differs in both the conduction and valence bands. The determination of the type of bandgap energy for 4-((2-hydroxy-3-methoxybenzylidene)amino)-N-(thiazol-2-yl)benzene sulfonamide is achieved through a comparison between the UV-visible bandgap energy and the Tauc plot, revealing that it falls under the category of indirect bandgap. The value of m is contingent upon the type of semiconductor bandgap energy and encompasses four distinct values: 3/2 for forbidden transition, 3 for forbidden indirect transition, 2 for allowing indirect transition [32]:

$$(\alpha h\nu) = A^* (h\nu - E_g)^2 . \quad (2)$$

Various methods can be employed to determine the bandgap energy, including Tauc plot, the first derivation of absorbance, and transmittance. For the 4-((2-hydroxy-3-methoxybenzylidene) amino)-N-(thiazol-2-yl)benzene sulfonamide molecule, the Tauc plot emerges as the most effective approach for calculating the bandgap energy (E_g). The values of E_g obtained through the Tauc plot method exhibit high similarity with those derived from the UV-visible spectra. Specifically, the E_g values, according to the Tauc plot method, are found to be 3.03, 3.18, 3.23 eV at one set of conditions and 3.02, 3.15, 3.16 eV at another set of conditions, corresponding to temperatures of 30 and 40 °C, as illustrated in Fig. 4.

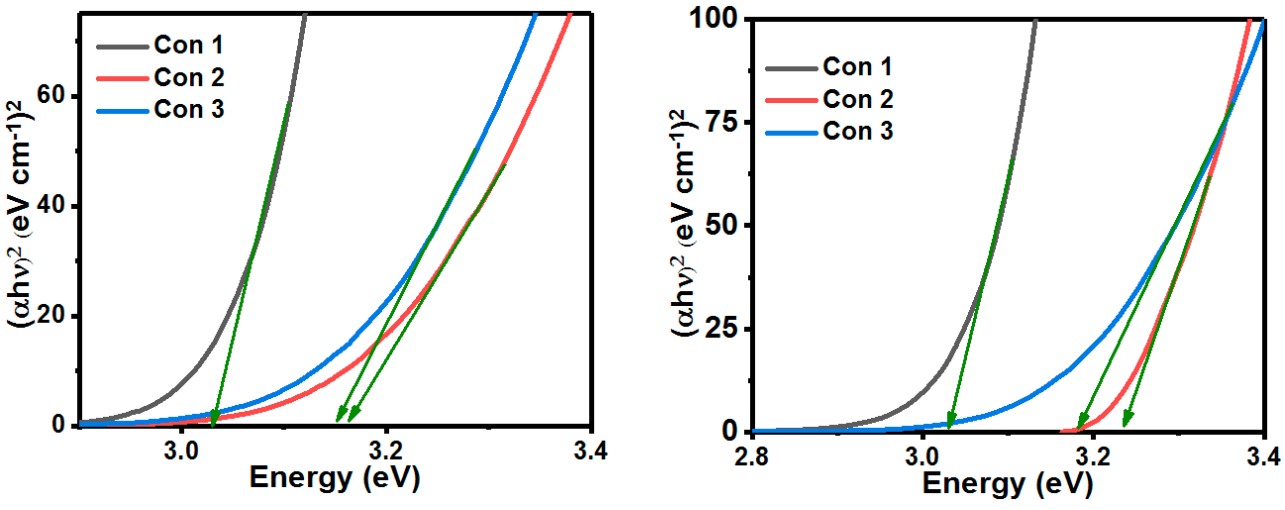

a b

Fig. 4. Tauc-plot of 4-((2-hydroxy-3-methoxybenzylidene) amino)-N-(thiazol-2-yl) benzene sulfonamide in DMSO (A) at 303.15 K and (B) at 313.15 K

3.1. Refractive index

The refractive index of semiconductor materials holds considerable importance in determining various parameters, including electronegativity, bandgap energy, electrical and optical conductivity, and dielectric constant. The performance of devices is contingent on the refractive index, making it a crucial factor in optoelectronic applications and technologies. The refractive index, denoted by the symbol n, can be obtained from the following expression [33]:

$$n = \left\{ \left[\frac{4R}{(R-1)^2} - k^2 \right]^{\frac{1}{2}} - \frac{R+1}{R-1} \right\}. \quad (3)$$

The characterization of semiconducting materials, fundamental to their optical and electrical properties, relies on two key parameters: energy gap and refractive index. The refractive index (n) is a descriptor of transparency to incident photons, while the energy gap (E_g) is determined by the threshold of photon absorption in a semiconductor. Various relationships exist between E_g and n, including those formulated by Moss, Ravindra, Hervé and Vandamme, as well as Reddy and Kumar, and Singh. The Moss and semi-empirical correlations, established as early as the 1950s, have been subjects of intensive study in subsequent years. These relationships play a crucial role in understanding and characterizing the optical and electrical properties of semiconducting materials [34–37].

Reddy relation:

$$n^4 \left(E_g - 0.365 \right) = 154 . \quad (4)$$

Moss relationship:

$$n^4 E_g = 95 \text{ eV}. \quad (5)$$

Ravindra relationship:

$$n = 4.084 - 0.62 E_g . \quad (6)$$

From the following equation of Tripathy, the relationship can calculate the refractive index:

$$n = n_0 \left[1 + \alpha e^{-\beta E_g} \right]. \quad (7)$$

Where, α, β and n_0 are constants which are equal to 1.9017, 0.539 eV^{-1} and 1.37 respectively.

Herve–Vandamme relationship:

$$n^2 = 1 + \left(\frac{A}{E_g + B} \right)^2 . \quad (8)$$

Kumar and Singh relations:

$$n = K E_g^c . \quad (9)$$

Where, K and C are constants which are equal to 3.3668 and –0.32234.

The refractive index (n) is a crucial parameter in the characterization of physical and chemical properties of materials, forming the basis for transparency measurements. Accurate knowledge of n is essential for designing optoelectronic devices due to its influence on electronic characteristics and the band structure of materials. In the case of the 4-((2-hydroxy-3-methoxybenzylidene)amino)-N-(thiazol-2-yl) benzene sulfonamide molecule, the refractive index is illustrated in Fig. 5. Experimental n values exhibit the lowest value compared to other relationships. Initially, the change in refractive index follows an approximately linear trend. Subsequently, n increases from 3.3 to 4.25 eV before decreasing to its initial position. At 6.19 eV, n is observed to be 0.18, with this value coinciding with the experimental and Ravindra relationship values. While each relationship has its unique characteristics, the Reddy relationship generally demonstrates the best compatibility with the refractive index. However, as the band gap exceeds 4 eV, the Moss relationship aligns more closely with experimental refractive index values. This relationship, for instance, at 6.2 eV, provides a closer match with experimental data in the middle to moderately high energy gap range. Nevertheless, it is noted that the Moss equation is inaccurate for materials with a band gap less than 0.365 eV [38]. The applicability of these relationships is contingent on the material type and bandgap energy. For instance, the Kumar & Singh relationship is more suitable for semiconductor binaries compared to other materials.

Moss's determination reveals that electron energy levels are scaled down by the effective dielectric constant, experienced by the electron within the material, based on photoconductivity [39]. The dielectric constant of materials is approximately proportional to the square of the

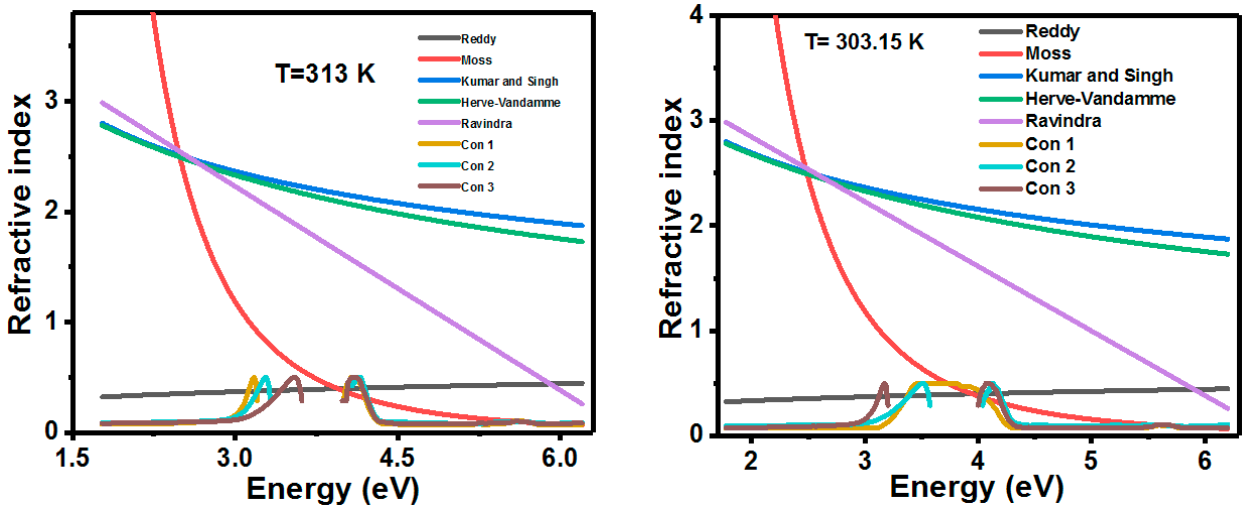

Fig. 5. Variation of refractive index of different relations with bandgap energy of 4-((2-hydroxy-3-methoxybenzylidene) amino)-N-(thiazol-2-yl) benzene sulfonamide molecule in DMSO solvent

refractive index. The Ravindra relation, used to calculate the refractive index for semiconductors, assumes a linear relationship in energy gap, postulating that the valence and conduction bands are more or less parallel to each other along symmetry directions[40]. This model posits a constant difference between UV resonance energy and the energy gap, based on oscillatory theory assumptions. In the context of the 4-((2-hydroxy-3-methoxybenzylidene)amino)-N-(thiazol-2-yl)benzene sulfonamide molecule in DMSO, the Kumar and Singh relationship yields a refractive index (n) value of 2.33. This model describes n as governed by an energy law behavior with respect to the energy gap, and the model parameters are fitted to experimental energy gaps and refractive index data. Moss's calculation for n in DMSO results in the highest value in this study, reaching 4.856 as presented in Table 2. The refractive index is influenced by the wavelength of light and the concentration in the solution. The relationship between temperature and the refractive index of molecules is explained by the refractive index remaining unaffected by temperature changes but varying due to alterations in density. With increasing temperature, materials typically expand, leading to a decrease in density. However, if the material undergoes compression, the density remains constant despite temperature changes. Notably, altering pressure does not induce changes in the refractive index [41–43].

Dispersion is a crucial parameter for comprehending the physical properties of materials, particularly how light bends at specific wavelengths. In Fig. 6, the Normal dispersion region of the 4-((2-hydroxy-3-methoxybenzylidene) amino)-N-(thiazol-2-yl)benzene sulfonamide molecule in DMSO is calculated by considering the relationship between the refractive index and angular frequency. The scattering area is a key property for designing optical pigments. As the angular frequency increases, the refractive index may fluctuate, leading to an expansion of the scattering area. Utilizing the refractive index and Normal dispersion area in the design of multi-element systems is highly valuable, enabling designers to precisely predict how light will behave throughout the entire optical path.

Table. 2. The average value of refractive indices of the 4-((2-hydroxy-3-methoxybenzylidene)amino)-N-(thiazol-2-yl) benzene sulfonamide molecule in DMSO for various relations and experimental

Moss	Reddy	Herve-Vandamme	Ravindra	Kumar and Singh	T = 303.15 K			T = 313.15 K		
					Concentration					
					1	2	3	1	2	3
4.856	0.3831	2.25505	1.62242	2.336455	0.0866	0.0706	0.0918	0.0738	0.0856	0.082

3.2. Reflectivity and reflection loss

The optical response of a material's surface can be assessed through the reflectivity coefficient, which is defined as the ratio of reflected power to incident power. This coefficient holds significance in understanding the optical properties of materials. The reflectivity can be calculated in terms of the extinction coefficient and refractive index, and this relationship is expressed as follows [44, 45]:

$$R = \frac{(n-1)^2 + k^2}{(n+1)^2 + k^2}. \quad (10)$$

Where k is represent the frequency-dependent extinction coefficient, for a weak absorber k can be considered too small and at the high frequency it vanishes. The following expression can calculate the reflectivity at a higher frequency:

$$R = \left(\frac{n-1}{n+1}\right)^2. \quad (11)$$

The relation between reflectivity and reflection coefficient can determine the reflection coefficient:

$$r = \sqrt{R}. \quad (12)$$

The reflectivity exhibits its highest values at both the lowest and highest bandgap energies, as depicted in Figures 6 and 7. During the maximum absorption of light within the range of 3.2 to 3.9 eV for both temperature conditions, the reflectivity reaches its lowest values, indicating minimal reflection of light. At lower temperatures, the reflectivity is smaller compared to higher temperatures, which could be attributed to the expansion of the particle interiors within the

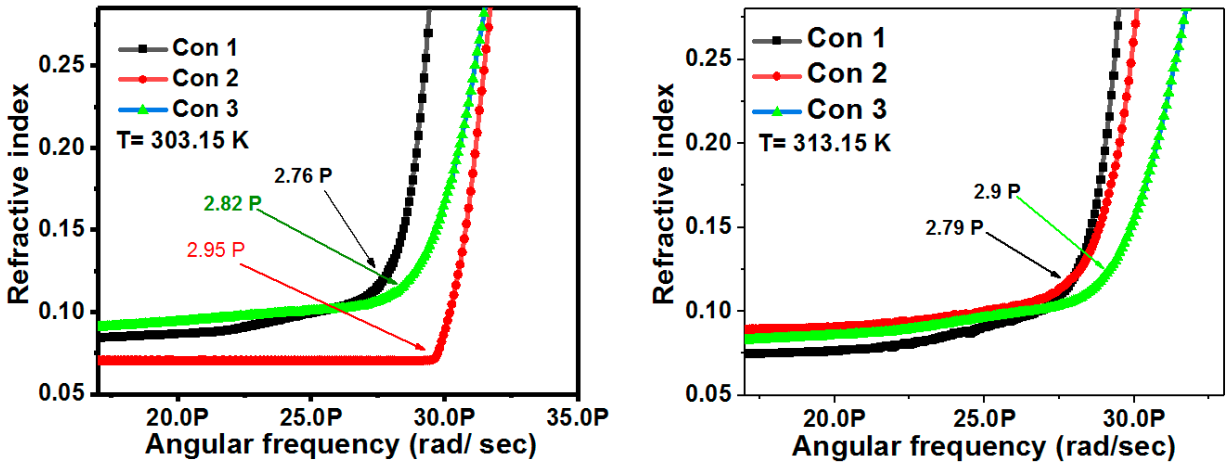

Fig. 6. Normal dispersion region of 4-((2-hydroxy-3-methoxybenzylidene) amino)-N-(thiazol-2-yl) benzene sulfonamide molecule in DMSO

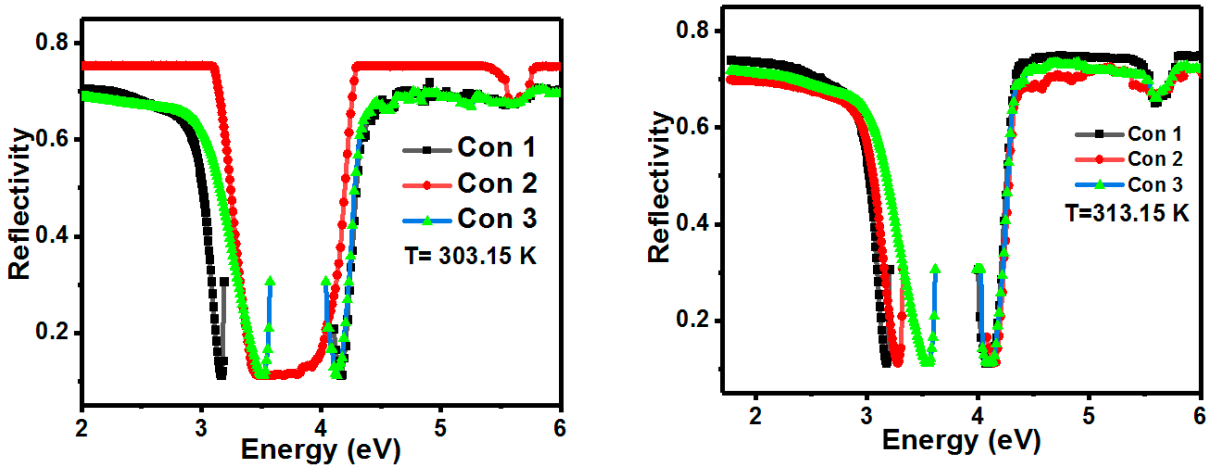

Fig. 7. Variation of reflectivity with bandgap energy of 4-((2-hydroxy-3-methoxybenzylidene) amino)-N-(thiazol-2-yl) benzene sulfonamide molecule in DMSO

molecule and the vibrational motion of atoms. As the aggregation proceeds, the medium becomes more turbid, leading to an increase in light absorption. By considering the ratio of the stability of these measurements to the constant aggregation rate *k*, the absorbance of photon energy is enhanced.

The optical behavior of semiconductor materials at very low frequencies exhibits characteristics akin to metals, while at high frequencies, they resemble insulators. The plasma frequency serves as a characteristic frequency at which the material transitions from a metallic to a dielectric response[46]. According to the Drude model, the plasma frequency is defined as frequency at which the real part of the dielectric function vanishes $\varepsilon_r(w_p)=0$.

Refractive index and absorption coefficient (*k*) are the same at a low frequency while *k* and *n* are large. The following equation can describe the Normal reflectivity [47]:

$$R=\frac{(n-1)^2+k^2}{(n+1)^2+k^2}=\frac{n^2+k^2-2n}{n^2+k^2+2n}= \\ =1-\frac{4n}{n^2+k^2}\approx 1-\frac{2}{n}. \quad (13)$$

A material with a large concentration at low frequency acts as a perfect reflector. The sharpness of the plasma structure, determined by the relaxation time at the plasma frequency, is indicative of a longer relaxation time when the plasma structure is sharper. The absorption property is crucial due to its relationship with electrical and optical properties through the conductivity tensor. A material that is a good electrical conductor exhibits high reflection, while transparent materials are generally expected to have reasonably poor electrical conductivity [48].

4. Optical and electrical conductivity

The electrical and optical conductivity of semiconductor materials is very significant for the investigation of the variation of conductivity with bandgap energy. From the following expressions can calculate both of them [49]:

$$\sigma_{opt}=\frac{\alpha nc}{4\pi}, \quad (13)$$

$$\sigma_{ele}=\frac{2\lambda\sigma_{opt}}{\alpha}. \quad (14)$$

Here, λ is the wavelength of the incident light, *c* is the velocity of light and α is the absorption coefficient.

Figs. 8 a and b show the photoconductivity variation at 303.15 and 313.15 K for three different concentrations in the range of 3.4 to 3.8 eV. The optical conductivity has the lowest value due to the lack of light absorption. At 3.2 and 3.9 eV, it has the highest value corresponding to the maximum absorption as mentioned in Fig. 3. From the explanation in Fig. 8c and d, when an increase in temperature leads to an increase in conductivity and a decrease in resistance. The electrons in the valence band get excited and jump into the conduction band from HOMO (highest occupied molecular orbital) to LUMO (lowest unoccupied molecular orbital) in the case of semiconductors as the temperature increases. Hence, resulting in the dwindling of resistance the conductance increases. The resistivity and conductivity increase, and the reciprocal of conductivity decreases.

5. Dielectric constant

The dielectric constant of compounds plays a significant role in determining the conduction properties of the material. The electrical properties of a material are influenced by various factors, including different growth parameters such as deposition rate, substrate temperature, thickness, and film composition. The application of thin films for photovoltaic applications depends on the electrical properties of the materials, making it crucial for determining their suitability for specific applications. The dielectric constant can be calculated using the following expression [50]:

$$\varepsilon^{*}=\varepsilon'+j\varepsilon''. \quad (16)$$

Where the two parameters ε′ and ε″ represent the real part dielectric constant and imaginary part (dielectric loss), respectively. The grain, charge storage capabilities of dielectric material, grain boundary, grain, insights into the structure of compounds and transport properties are related to the dielectric spectroscopy of materials that is very significant. The potential barrier generates at the grain boundaries, and

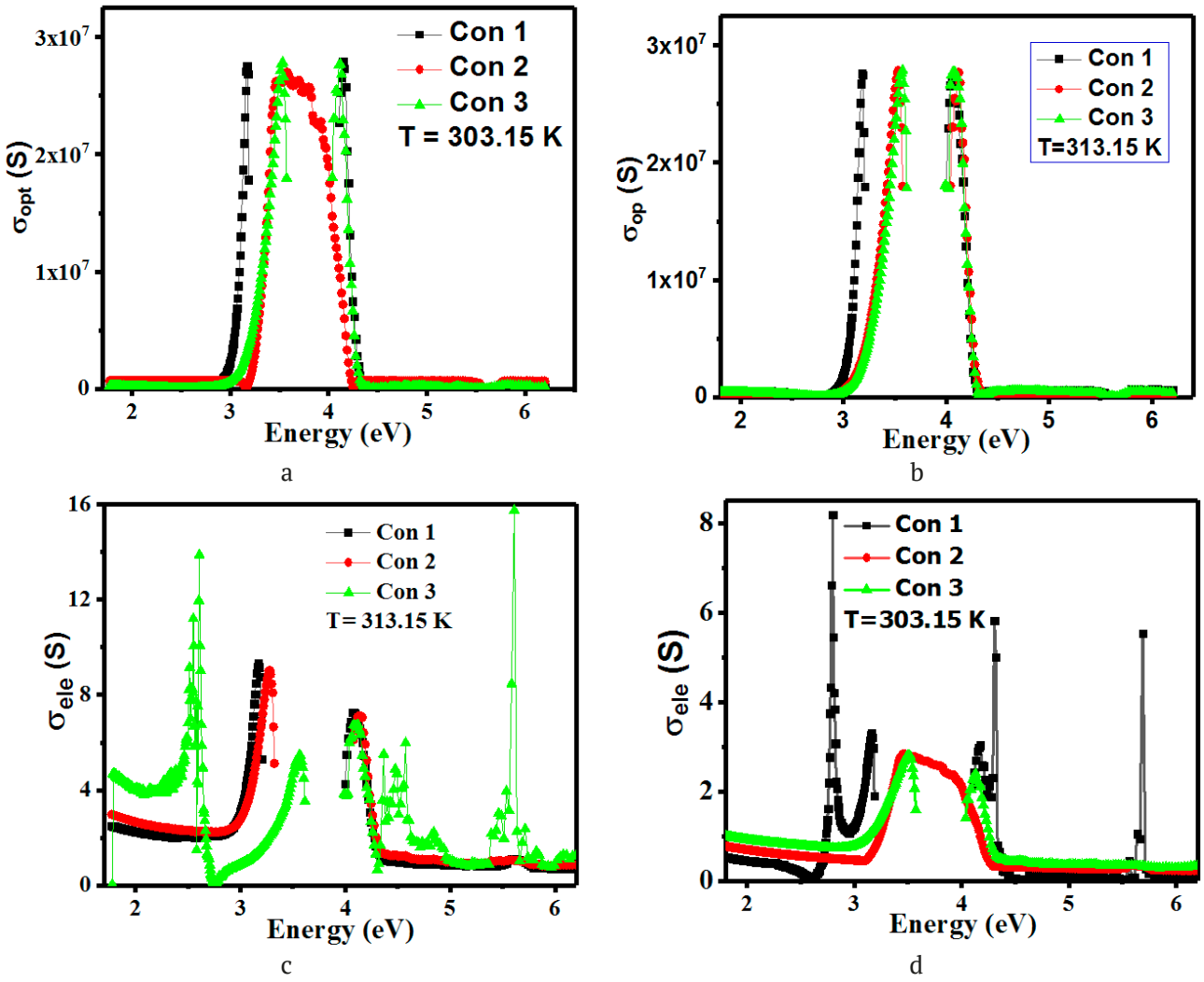

Fig. 8. Optical and electrical conductivity of 4-((2-hydroxy-3-methoxybenzylidene) amino)-N-(thiazol-2-yl) benzene sulfonamide molecule in DMSO

due to the presence of charge polarization, the dielectric constant increases with increased frequency [51].

At a specific frequency, the permittivity or dielectric constant represents the relationship between the electric field vector and the electric displacement vector. It's noteworthy that the dielectric constant can assume negative values at certain frequency bands, such as in plasmas at radio frequencies or metals at infrared frequencies. In Fig. 9, the real part of the dielectric constant is shown as negative, indicating negative permittivity, where the electric displacement vector and the electric field vector are in opposite directions. However, this negative value does not necessarily imply that the electrical energy stored in this medium is negative. The dielectric constant of materials depends on the molecular structure. Whether the dielectric constant increases or decreases during a given phase change relies on the specific phases involved, and the dielectric constant can exhibit sudden changes at phase boundaries with variations in temperature, as illustrated in Fig. 9.

6. Electronic structure

Based on density functional theory at the B3LYP level of theory with 6-311G ++ (*d*, *p*), quantum chemical calculations were carried out with the complete geometry optimizations of the chosen molecule [52]. The quantum chemical parameters from the HOMO and LUMO were performed. This study is to investigate the molecular properties regarding the reactivity and

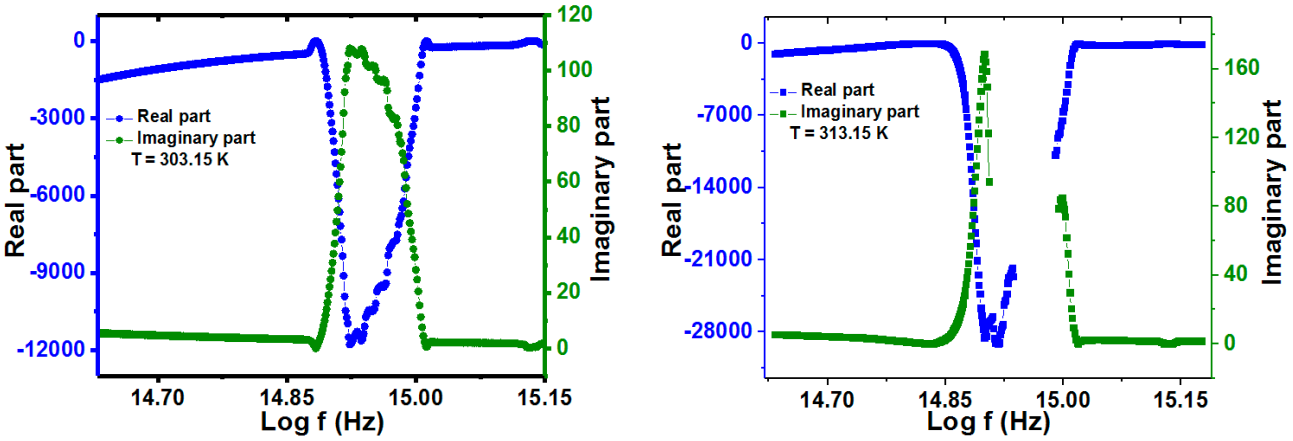

Fig. 9. Dielectric constant, real and imaginary part of 4-((2-hydroxy-3-methoxybenzylidene) amino)-N-(thiazol-2-yl) benzene sulfonamide molecule in DMSO at the second concentration associated with Table 1

selectivity of the compounds, they were estimated by Koopmans theory which related to HOMO (E_{HOMO}) and LUMO (E_{LUMO}) energy [53, 54].

Many quantitative chemical parameters such as ionization energy (I) and electron affinity (A) can be calculated. Ionization energy can be expressed in quantum computational chemistry and is the energy required to break an electron from a chemical species into a gas phase or isolated state. Based on Koopmans' theory, the ionization energies of chemical species are related to the HOMO energy which is the energy required to break an electron from HOMO. From the following equation can be calculated the ionization energy and is considered as the opposite sign of HOMO energy [55]:

$$I = -E_{HOMO}. \quad (17)$$

In the case of gas and isolated state, the change of electron energy absorption reaction of chemical species can be described by electron affinity. Electron affinity calculations are based on LUMO energy because in the basic type, the electron to be received will enter the lower-energy free orbital. Using Koopman's theorem, the electron affinity can be calculated for chemical species and is equal to the inverse sign of the LUMO energy:

$$A = -E_{LUMO}. \quad (18)$$

From the following equation, the bandgap energy of the particles can be calculated and is equal to the difference between E_{LUMO} and E_{HOMO}:

$$\Delta E = E_{LUMO} - E_{HOMO}. \quad (19)$$

The energy gaps are very different from each other in the intermolecular interaction such as the strong ionic interaction between molecules whose energy gap varies greatly. The energy gaps are very close to each other in the intermolecular interaction in strong covalent interaction. The hardness and softness property of molecules are useful parameters to describe chemical reactivity. Associate with corrosion inhibition efficiency, the soft molecule has a high inhibition efficiency than the hard molecule. Chemical hardness (η) and softness (σ) can be calculated using the following relation:

$$\eta = \frac{I - A}{2}, \quad (20)$$

$$\sigma = \frac{1}{\eta}. \quad (21)$$

Mulliken's electronegativity or absolute electronegativity is one of the essential factors that can calculate in quantum chemical computation, which is the arithmetic mean of ionization energy and electron affinity for species. The influential electron electrophiles or acceptors indicate the species with high electronegativity. The nucleophiles or donor electron represents low electronegativity. Mulliken electronegativity (χ) can be written as [56]:

$$\chi = \frac{I + A}{2}. \quad (22)$$

The calculated parameters for HOMO energy, LUMO energy, ionization energy (I), electron affinity (A), energy gap (ΔE), hardness (η), softness

(σ), electronegativity (χ), chemical potential (CP), electrophilicity index (*w*), Nucleophilicity (N), Back-donation energy (ΔE_{B-d}) and electron transferred (ΔN) are given in Table 3 for DMSO solvent. Fig. 10 shows HOMO and LUMO of DFT at 4-((2-hydroxy-3-methoxybenzylidene) amino)-N-(thiazol-2-yl) benzene sulfonamide molecule in DMSO and optimizing geometry performed at B3LYP level and the 6-311G ++ (d, p).

The theoretical and experimental values of bandgap energy agree well. The differences in E_g at different concentrations with temperature are slightly different from the theoretical. The electrophilicity index of this molecule has a high value and the molecule with a high electrophilicity index have more electron flux if they are involved in a transponder interaction and lower the energy more because of this electron flux

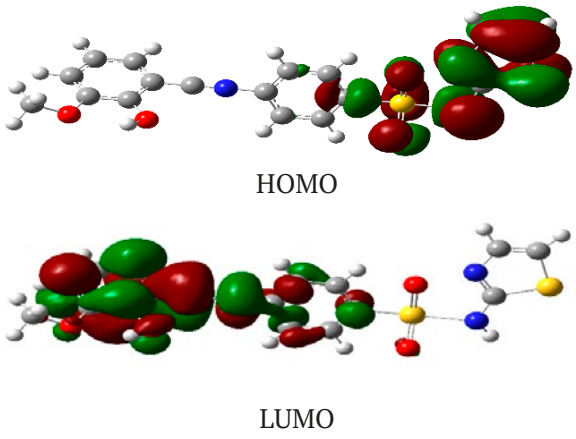

Fig. 10. HOMO and LUMO of DFT at 4-((2-hydroxy-3-methoxybenzylidene) amino)-N-(thiazol-2-yl) benzene sulfonamide molecule in DMSO and optimizing geometry performed at B3LYP level and the 6-311G ++ (d, p)

7. Electrostatic potential map

The charge distribution on the molecular surface is analyzed in three dimensions (X, Y, Z) through the molecule's electrical potential surface[57]. The Molecular Electrostatic Potential (MEP) allows for the visualization of variably charged regions on the molecule's surface, offering a valuable map to elucidate and discern chemical reactions and interactions with other molecules [58, 59]. This mapping is particularly useful in describing the characteristics of chemical bonds, commonly referred to as the "color code" section, as it vividly illustrates the charge distribution on the surface of Anthracene. Each color is distributed distinctively across the molecule's surface, and the geometry optimization was conducted at the B3LYP level with the 6-311G++ (d, p) basis set. In this color-coded representation, the red color signifies the presence of electrons, predominantly surrounding the sulfur bonds with O32 and O33 atoms, transitioning to yellow regions located between the carbon and hydrogen bonds. Hydrogen is distinctly depicted in green, denoting its lower electronegativity compared to red and yellow regions, as illustrated in Fig. 11. MEPs provide insights into the polarization range, with the molecule's electronegativity playing a significant role in determining the polarization of charges. The regions where colors do not intersect effectively help identify areas with high negative or positive charges. Notably,

Table. 3. Quantum computational parameters based on DFT at 4-((2-hydroxy-3-methoxybenzylidene) amino)-N-(thiazol-2-yl) benzene sulfonamide molecule in DMSO and optimizing geometry performed at (B3LYP) level and the 6-311G ++ (d, p)

E_{HOMO} (эВ)	E_{LUMO} (эВ)	ΔE (эВ)	I	A	η	σ	χ	CP	w	N	ΔE_{B-d}	ΔN
−5.40	−2.54	2.86	5.40	2.54	1.43	0.69	3.97	−3.9	5.51	0.18	−0.358	1.05

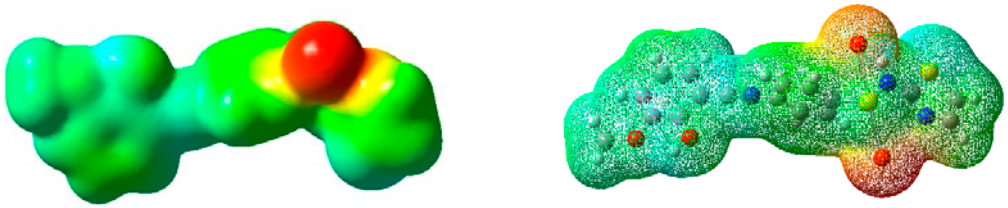

Fig. 11. Electrostatic potential map of 4-((2-hydroxy-3-methoxybenzylidene) amino)-N-(thiazol-2-yl) benzene sulfonamide molecule in DMSO based on DFT at 6-311G++ (d, p) basis set

negative potential sites are concentrated around the carbon resonant bonds of benzene rings. The molecular electrostatic potential map highlights a robust repulsion at positive potential sites on edge hydrogen atoms, while carbon bonds exhibit a compelling attraction.

8. Conclusion

The optical characteristics of the 4-((2-hydroxy-3-methoxybenzylidene)amino)-N-(thiazol-2-yl)benzene sulfonamide molecule in DMSO were systematically examined in this study. It was observed that the bandgap energy of the molecule could be manipulated by adjusting its concentration. Notably, the practical refractive index, determined in comparison to other relationships, exhibited its lowest value. The investigation also revealed that temperature exerts an influence on the spatial arrangement of atoms, forming the molecular structure. As temperature increases, the optical density of the sample medium decreases due to enhanced atomic vibration, leading to an expansion of interatomic distances. Consequently, the medium becomes less optically dense, resulting in a higher velocity of light and a lower refractive index, causing a slight alteration in the deflection angle at elevated temperatures. While the optical conductivity showed marginal differences, the electrical conductivity demonstrated higher values and variations at elevated temperatures. Additionally, based on Density Functional Theory (DFT) calculations, the molecule exhibited lower softness and higher global hardness in the DMSO solvent. The electrophilic and nucleophilic parameters, vital for describing electron-deficient (electrophilic) and electron-rich (nucleophile) species, indicated a high electrophilic value and a low nucleophilic value for this molecule.

Author contributions

All authors made an equivalent contribution to the preparation of the publication.

Conflict of interest

The authors declare no conflict of interest.

References

1. Shafiee A., Ghadiri E., Kassis J., Williams D., Atala A. Energy band gap investigation of biomaterials: A comprehensive material approach for biocompatibility of medical electronic devices. *Micromachines*. 2020;11(1): 105. https://doi.org/10.3390/mi11010105

2. Mamand D. M., Qadr H. M. Density functional theory and computational simulation of the molecular structure on corrosion of carbon steel in acidic media of some amino acids. *Russian Journal of Physical Chemistry A*. 2022;96: 2155–2165. https://doi.org/10.1134/s0036024422100193

3. Qadr H. M., Mamand D. Measuring energy loss of alpha particles in hydrogen gas. *El-Cezeri Fen ve Mühendislik Dergisi*. 2023;10: 433–438. https://doi.org/10.31202/ecjse.1195041

4. Vieira D. F., Avellaneda C. O., Pawlicka A. Conductivity study of a gelatin-based polymer electrolyte. *Electrochimica Acta*. 2007;53: 1404–1408. https://doi.org/10.1016/j.electacta.2007.04.034

5. Fujita S.-I., Kawamori H., Honda D., Yoshida H., Arai M. Photocatalytic hydrogen production from aqueous glycerol solution using NiO/TiO_2 catalysts: Effects of preparation and reaction conditions. *Applied Catalysis B: Environmental*. 2016;181: 818–824. https://doi.org/10.1016/j.apcatb.2015.08.048

6. Nan H., Ping Y., Xuan C., ... Tingfei, X. Blood compatibility of amorphous titanium oxide films synthesized by ion beam enhanced deposition. *Biomaterials*. 1998;19(7-9): 771–776. https://doi.org/10.1016/s0142-9612(98)00212-9

7. Qadr H. M. A Molecular dynamics study of temperature dependence of the primary state of cascade damage processes. *Russian Journal of Non-Ferrous Metals*. 2021;62: 561-567. https://doi.org/10.3103/s1067821221050096

8. Abram R. A., Childs G. N., Saunderson P. A. Band gap narrowing due to many-body effects in silicon and gallium arsenide. *Journal Of Physics C: Solid State Physics*. 1984;17: 6105. https://doi.org/10.1088/0022-3719/17/34/012

9. Hudgins J. L., Simin G. S., Santi E., Khan M. A. An assessment of wide bandgap semiconductors for power devices. *Ieee Transactions On Power Electronics*. 2003;18: 907–914. https://doi.org/10.1109/tpel.2003.810840

10. Rawal S. B., Bera S., Lee D., Jang D.-J., Lee W. I. Design of visible-light photocatalysts by coupling of narrow bandgap semiconductors and TiO_2: Effect of their relative energy band positions on the photocatalytic efficiency. *Catalysis Science & Technology*. 2013;3: 1822–1830. https://doi.org/10.1039/c3cy00004d

11. Örek C., Arslan F., Gündüz B., Kaygili O., Bulut N. Comparison of experimental photonic and refractive index characteristics of the TBADN films with their theoretical counterparts. *Chemical Physics Letters*. 2018;696: 12-18. https://doi.org/10.1016/j.cplett.2018.02.035

12. Orek C., Gündüz B., Kaygili O., Bulut N. Electronic, optical, and spectroscopic analysis of TBADN organic semiconductor: Experiment and theory. *Chemical Physics Letters*. 2017;678: 130–138. https://doi.org/10.1016/j.cplett.2017.04.050

13. Mohan S., Kato E., Drennen Iii J. K., Anderson C. A. Refractive index measurement of pharmaceutical solids: A review of measurement methods and pharmaceutical applications. *Journal of Pharmaceutical Sciences*. 2019;108: 3478–3495. https://doi.org/10.1016/j.xphs.2019.06.029

14. Qadr H. M. Investigation of gamma ray buildup factor for some shielding absorber. *Cumhuriyet Science Journal*. 2022;43: 520–525. https://doi.org/10.17776/csj.1098571

15. Chaudhary A., Nagaich U., Gulati N., Sharma V. K., Khosa R. L., Partapur M. U. Enhancement of solubilization and bioavailability of poorly soluble drugs by physical and chemical modifications: A recent review. *Journal of Advanced Pharmacy Education and Research*. 2012;2: 32–67.

16. Al-Otaibi J. S., Mary Y. S., Thomas R., Kaya S. Detailed electronic structure, physico-chemical properties, excited state properties, virtual bioactivity screening and sers analysis of three guanine based antiviral drugs valacyclovir HCl hydrate, acyclovir and ganciclovir. *Polycyclic Aromatic Compounds*. 2022;42: 1260–1270. https://doi.org/10.1080/10406638.2020.1773876

17. Mamand D. M., Awla A. H., Anwer T. M. K., Qadr H. M. Quantum chemical study of heterocyclic organic compounds on the corrosion inhibition. *Chimica Techno Acta*. 2022;9: 20229203. https://doi.org/10.15826/chimtech.2022.9.2.03

18. Qadr H. M. Effect of ion irradiation on the mechanical properties of high and low copper. *Atom Indonesia*. 2020;46: 47–51. https://doi.org/10.17146/aij.2020.923

19. Zhang J., Tang H., Liu Z., Chen B. Effects of major parameters of nanoparticles on their physical and chemical properties and recent application of nanodrug delivery system in targeted chemotherapy. *International Journal of Nanomedicine*. 2017;12: 8483. https://doi.org/10.2147/ijn.s148359

20. Qadr H. M. A molecular dynamics calculation to cascade damage processes. *The Annals of "Dunarea de Jos" University of Galati. Fascicle IX, Metallurgy and Materials Science*. 2020;43: 13–16. https://doi.org/10.35219/mms.2020.4.02

21. Sechadri S., Rasheed M. P., Sangeetha R. Molecular structure, spectroscopic (FTIR, FT-Raman, 13C and 1H NMR, UV), polarizability and first-order hyperpolarizability, HOMO–LUMO analysis of 2,4-difluoroacetophenone. *Spectrochimica Acta Part A: Molecular and Biomolecular Spectroscopy*. 2015;7: 56–70. https://doi.org/10.1016/j.saa.2014.09.069

22. Aziz D. M., Azeez H. J. Synthesis of new β-lactam-N-(thiazol-2-yl)benzene sulfonamide hybrids: Their in vitro antimicrobial and in silico molecular docking studies. *Journal of Molecular Structure*. 2020;1222: 128904. https://doi.org/10.1016/j.molstruc.2020.128904

23. Brisdon A. K. *Inorganic spectroscopic methods*. New York: Oxford University Press; 1998. https://doi.org/10.1093/hesc/9780198559498.001.0001

24. Coskun D., Gunduz B., Coskun M. F. Synthesis, characterization and significant optoelectronic parameters of 1-(7-methoxy-1-benzofuran-2-yl) substituted chalcone derivatives. *Journal of Molecular Structure*. 2019;1178: 261–267. https://doi.org/10.1016/j.molstruc.2018.10.043

25. Choi W. S., Yoon J.-G. Optical characterization of band gap graded ZnMgO films. *Solid State Communications*. 2012;152: 345–348. https://doi.org/10.1016/j.ssc.2011.12.019

26. Tsukazaki A., Akasaka S., Nakahara K., ... Kawasaki M. Observation of the fractional quantum Hall effect in an oxide. *Nature Materials*. 2010;9: 889–893. https://doi.org/10.1038/nmat2874

27. Garimella S. V., Persoons T., Weibel J. A., Gektin V. Electronics thermal management in information and communications technologies: Challenges and future directions. *IEEE Transactions on Components, Packaging and Manufacturing Technology*. 2016;7: 1191–1205. https://doi.org/10.1109/tcpmt.2016.2603600

28. Trew R. J. Wide bandgap semiconductor transistors for microwave power amplifiers. *IEEE Microwave Magazine*. 2000;1: 46–54. https://doi.org/10.1109/6668.823827

29. Neudeck P. G., Okojie R. S., Chen L.-Y. High-temperature electronics - a role for wide bandgap semiconductors? *Proceedings of The Ieee*. 2002;90: 1065–1076. https://doi.org/10.1109/jproc.2002.1021571

30. Mamand D. M., Anwer T. M. K., Qadr H. M. Theoretical investigation on corrosion inhibition effect of oxadiazole: Dft calculations. *Oxidation Communications*. 2022;45: 600-267.

31. Mamand D. M., Qadr H. M. Corrosion inhibition efficiency of quinoxalines based on electronic structure and quantum computational analysis. *Revue Roumaine de Chimie*. 2023;68: 435–446.

32. Cassabois G., Valvin P., Gil B. Hexagonal boron nitride is an indirect bandgap semiconductor. *Nature Photonics*. 2016;10: 262–266. https://doi.org/10.1038/nphoton.2015.277

33. Mamand D. M., Anwer T. M., Qadr H. M., Mussa C. H. Investigation of spectroscopic and optoelectronic properties of phthalocyanine molecules. *Russian Journal of General Chemistry*. 2022;92: 1827–1838. https://doi.org/10.1134/s1070363222090249

34. Schütz A., Günthner M., Motz G., Greißl O., Glatzel U. Characterisation of novel precursor-derived ceramic coatings with glass filler particles on steel substrates. *Surface and Coatings Technology*. 2012;207: 319–327. https://doi.org/10.1016/j.surfcoat.2012.07.013

35. Tripathy S. K. Refractive indices of semiconductors from energy gaps. *Optical Materials*. 2015;46: 240–246. https://doi.org/10.1016/j.optmat.2015.04.026

36. Qadr H. M., Mamand D. M. A Computational study of substituent effect 1, 3, 4-thiadiazole on corrosion inhibition. *Azerbaijan Chemical Journal*. 2023; 19–29. https://doi.org/10.32737/0005-2531-2023-2-19-29

37. Mamad D. M., Omer P. K., Rasul H. H., Qadr H. M. A Theoretical study of structure and corrosion inhibition of some heterocyclic imidazoles: DFT investigation. *Surface Engineering and Applied Electrochemistry*. 2023;59: 489–501. https://doi.org/10.3103/s1068375523040099

38. Mamad D. M., Qadr H. M. Quantum computations and density functional theory on corrosion inhibition efficiency of BIA, HBT, MBI and PIZ compounds. *Himia, Fizika ta Tehnologia Poverhni*. 2023;14: 159–172. https://doi.org/10.15407/hftp14.02.159

39. Herve P., Vandamme L. K. J. General relation between refractive index and energy gap in semiconductors. *Infrared Physics & Technology*. 1994;35: 609–615. https://doi.org/10.1016/1350-4495(94)90026-4

40. Reddy R. R., Ahammed Y. N. A study on the Moss relation. *Infrared Physics & Technology*. 1995;36: 825–830. https://doi.org/10.1016/1350-4495(95)00008-m

41. Ravindra N. M., Ganapathy P., Choi J. Energy gap–refractive index relations in semiconductors – An overview. *Infrared Physics & Technology*. 2007;50: 21–29. https://doi.org/10.1016/j.infrared.2006.04.001

42. Aly K. M., Esmail E. Refractive index of salt water: effect of temperature. *Optical Materials*. 1993;2: 195–199. https://doi.org/10.1016/0925-3467(93)90013-q

43. Mamand D. M., Qadr H. M. Corrosion inhibition efficiency and quantum chemical studies of some organic compounds: theoretical evaluation. *Corrosion Reviews*. 2023;41: 427–441. https://doi.org/10.1515/corrrev-2022-0085

44. Wesely M. L. The combined effect of temperature and humidity fluctuations on refractive index. *Journal of Applied Meteorology*. 1976; 43–49. https://doi.org/10.1175/1520-0450(1976)015<0043:tceota>2.0.co;2

45. Mamand D. M., Azeez Y. H., Qadr H. M. Monte Carlo and DFT calculations on the corrosion inhibition efficiency of some benzimide molecules. *Mongolian Journal Of Chemistry*. 2023;24: 1–10. https://doi.org/10.5564/mjc.v24i50.2435

46. Tripathy S. K., Pattanaik A. Optical and electronic properties of some semiconductors from energy gaps. *Optical Materials*. 2016;53: 123–133. https://doi.org/10.1016/j.optmat.2016.01.012

47. Dresselhaus M. S. *Solid State Physics part II Optical properties of solids*. Lecture Notes. Massachusetts Institute of Technology, Cambridge, Ma; 2001;17: 15–16.

48. Patterson J. D., Bailey B. C., Patterson J. D., Bailey B. C. Optical properties of solids. In: *Solid-State Physics*. Springer, Cham.; 2018. 649–704. https://doi.org/10.1007/978-3-319-75322-5_10

49. Dalven R. *Introduction to applied solid state physics: Topics in the applications of semiconductors, superconductors, ferromagnetism, and the nonlinear optical properties of solids*. Springer Science & Business Media; 2012.

50. Dong H. M., Zhang J., Peeters F. M., Xu W Optical conductance and transmission in bilayer graphene. *Journal of Applied Physics*. 2009;106: 043103. https://doi.org/10.1063/1.3200959

51. Yücedağ I., Altındal Ş., Tataroğlu A. On the profile of frequency dependent series resistance and dielectric constant in MIS structure. *Microelectronic Engineering*. 2007;84: 180–186. https://doi.org/10.1016/j.mee.2006.10.071

52. Dege N., Gökce H., Doğan O. E., ... Sert Y. Quantum computational, spectroscopic investigations on N-(2-((2-chloro-4,5-dicyanophenyl)amino)ethyl)-4-methylbenzenesulfonamide by DFT/TD-DFT with different solvents, molecular docking and drug-likeness researches. *Colloids And Surfaces A: Physicochemical and Engineering Aspects*. 2022;638: 128311. https://doi.org/10.1016/j.colsurfa.2022.128311

53. Mamand D. M., Qadr H. M. Comprehensive spectroscopic and optoelectronic properties of BBL organic semiconductor. *Protection of Metals and Physical Chemistry of Surfaces*. 2021;57: 943–53. https://doi.org/10.1134/s207020512105018x

54. Mamand D. M., Qadr H. M. Optoelectronic properties of benzimidazobenzophenanthroline thin film. *Russian Microelectronics*. 2023;52: 325–336. https://doi.org/10.1134/s1063739723700531

55. Qadr H. M., Mamand D. M. Molecular structure and density functional theory investigation corrosion inhibitors of some oxadiazoles. *Journal of Bio- and Tribo-Corrosion*. 2021;7: 140. https://doi.org/10.1007/s40735-021-00566-9

56. Putz M. V., Russo N., Sicilia E. About the Mulliken electronegativity in DFT. *Theoretical Chemistry Accounts*. 2005;114: 38–45. https://doi.org/10.1007/s00214-005-0641-4

57. Medimagh M., Mleh C. B., Issaoui N., ... Bousiakoug L. G.. DFT and molecular docking study of

the effect of a green solvent (water and DMSO) on the structure, MEP, and FMOs of the 1-ethylpiperazine-1,4-diium bis(hydrogenoxalate) compound. *Compound. Journal Of Molecular Liquids*. 2023;369: 120851. https://doi.org/10.1016/j.molliq.2022.120851

58. Ramalingam S., Babu P. D. S., Periandy S., Fereyduni E. Vibrational investigation, molecular orbital studies and molecular electrostatic potential map analysis on 3-chlorobenzoic acid using hybrid computational calculations. *Spectrochimica Acta Part A: Molecular and Biomolecular Spectroscopy*. 2011;84: 210–220. https://doi.org/10.1016/j.saa.2011.09.030

59. Mamand D. M., Rasul H. H., Omer P. K., Qadr H. M. Theoretical and experimental investigation on ADT organic semiconductor in different solvents. *Condensed Matter And Interphases*. 2022;24(2): 227–42. https://doi.org/10.17308/kcmf.2022.24/9263

Information about the authors

Dyari Mustafa Mamand, MSc in Atomic and Molecular Physics, Department of Physics, University of Raparin (Sulaymaniyah, Iraq).
https://orcid.org/0000-0002-1215-7094
dyari.mustafa@uor.edu.krd

Dara Muhammed Aziz, PhD in Organic Chemistry, Department of Chemistry, University of Raparin (Sulaymaniyah, Iraq).
https://orcid.org/0000-0003-3362-6301
darachem@uor.edu.krd

Hiwa Mohammad Qadr, MSc in Physics, Lecture of the Department of Physics, University of Raparin (Sulaymaniyah, Iraq).
https://orcid.org/0000-0001-5585-3260
hiwa.physics@uor.edu.krd

Received 24.02.2023; approved after reviewing 24.06.2023; accepted for publication 16.09.2023; published online 25.03.2024.